Monthly Notices
of the
ROYAL ASTRONOMICAL SOCIETY

MNRAS **429,** 652–660 (2013) doi:10.1093/mnras/sts370

# Multicolour time series photometry of three periodic ultracool dwarfs

Chris Koen★

*Department of Statistics, University of the Western Cape, Private Bag X17, Bellville, 7535 Cape, South Africa*

Accepted 2012 November 5. Received 2012 November 5; in original form 2012 September 2

**ABSTRACT**

Photometry in *I*, or contemporaneously in *I* and *R*, of the known variable ultracool dwarfs Kelu-1 and 2MASS J11553952−3727350 is presented. The nature of the variability of Kelu-1 appears to evolve on time-scales of a day or less. Both the period and amplitude of the variability of 2MASS J11553952−3727350 have changed substantially since publication of earlier observations of the object. DENIS 1454−6604 is a new variable ultracool dwarf, with persistent and prominent brightness modulations at a period of 2.6 h.

**Key words:** stars: brown dwarfs – stars: variables: general – stars: individual: Kelu-1, 2MASS J11553952-3727350, DENIS-P J145407.8-640447.

## 1 INTRODUCTION

This paper describes observations of the three ultracool (L-type) dwarfs Kelu-1 (2MASS J13054019−2541059), 2MASS J11553952−3727350 (hereafter 2M 1155−3727) and DENIS-P J145407.8−640447 (hereafter DENIS 1454−6604). The former two objects are known to be periodic variables (see respectively Clarke, Tinney & Covey 2002; Clarke, Tinney & Hodgkin 2003; Koen 2003) while the photometry below demonstrates that DENIS 1454−6604 is also a sinusoidal variable. Table 1 gives some pertinent information about the three ultracool dwarfs (UCDs). The aim of the project was to obtain extensive multicolour time series photometry of the three targets.

As mentioned above, 2M 1155−3727 and Kelu-1 are known variables. Koen (2003) found an 8 h period in *I*-band observations of the former object, while Clarke et al. (2002) discovered a 1.8 h periodicity ($f = 13.3\,\mathrm{d}^{-1}$) in Kelu-1, observing through a filter centred roughly at 8700 Å. Although later *I*-band observations of Kelu-1 by Clarke et al. (2003) did find the object again to be variable, the brightness changes appeared to be aperiodic. Nonetheless, spectroscopy obtained a few nights earlier showed the H$\alpha$ equivalent width varying with $P \sim 1.8$ h. The 1.8 h period was also confirmed by Littlefair et al. (2006) in the $g'$ band, but simultaneous photometry through a narrow-band filter centred on 5900 Å showed no variability.

Liu & Leggett (2005) and Gelino et al. (2006) independently discovered that Kelu-1 is in fact a binary, with component spectral types of L2 and L3.5, according to the latter authors. The orbital period is of the order of 40 yr or longer, and the orbital inclination in excess of 81°. Both sets of authors measured a distance on the sky of about 0.29 arcsec between the components. Given this small separation all the photometry of the binary reported below includes both components.

★E-mail: ckoen@uwc.ac.za

Several attempts have been made to measure radio emission from Kelu-1, with null results (Berger 2006; Audard et al. 2007; Antonova et al. 2008), but X-ray radiation was detected by Audard et al. (2007).

Further optical photometry of Kelu-1 ($V = 21.8$, $R_c = 19.10$) was published by Dahn et al. (2002) and by Liebert & Gizis (2006; $R = 19.1$, $I = 16.9$). Mid-infrared photometry of Kelu-1 and 2M 1155−3727 is available in Patten et al. (2006). Recent proper motion measurements of the two objects were presented by Faherty et al. (2009, 2012). Its parallax of $104.4 \pm 4.7$ mas (Faherty et al. 2012) places 2M 1155−3727 at a mere $9.6 \pm 0.4$ pc from Earth. Zapatero Osorio, Caballero & Béjar (2005) detected polarization in Kelu-1, but this could not be confirmed in later observations by Goldman et al. (2009).

Section 2 below describes the experimental setup used to acquire the data analysed in Section 3. Concluding remarks are in Section 4.

## 2 THE OBSERVATIONS

The bulk of the observations were made with the South African Astronomical Observatory (SAAO) STE4 CCD camera, mounted on the SAAO 1.9 m telescope at Sutherland, South Africa. The camera is equipped with 1K × 1K chip, giving a field of view of about 2.5 arcmin × 2.5 arcmin. All observations were pre-binned 2 × 2, resulting in a readout time of about 20 s, and a pixel scale of 0.28 arcsec/pixel. The last two nights of monitoring of DENIS 1454−6604 made use of the SAAO STE3 camera, with similar properties to the STE4 camera, but with only a quarter of its field of view. Operated in the standard 2 × 2 pre-binning mode, readout time with this camera was only 5 s. An observing run typically consisted of continuous monitoring over several hours, alternating exposures of 1–3 min through Cousins *I* and *R* filters. Some runs used *I* only, and DENIS 1454−6604 was sometimes observed in *IZ* or even *RIZ*. A log of the observations is given in Table 2.

Photometric reductions were completely standard. Bias was determined from an overscan region, and subtracted from the image,

**Table 1.** Some basic information about the target objects. Optical and near-infrared photometry is from the DENIS (Epchtein et al. 1999) and 2MASS (Skrutskie et al. 2006) catalogues, respectively. Numbers in parentheses are the keys to other sources of information: (1) – Gelino, Kulkarni & Stephens (2006); (2) – Gizis (2002); (3) – Phan-Bao et al. (2008); (4) – Mohanty & Basri (2003); (5) – Reiners & Basri (2008); (6) – Clarke et al. (2003); (7) – Basri et al. (2000); (8) – Blake, Charbonneau & White (2010).

| Name | $I$ | $J$ | $I-J$ | Spectrum | H$\alpha$ EW (Å) | $v \sin i$ (km s$^{-1}$) |
|---|---|---|---|---|---|---|
| Kelu-1 | 16.85 | 13.41 | 3.44 | L2+L3.5 (1) | 1.5 (4); 1.75 (5); 1.4–4.4 (6) | 60 (7); 76 (5) |
| 2M 1155−3727 | 16.18 | 12.81 | 3.37 | L2 (2) | 2.5 (2); 1–2.4 (5) | 22 (5); 13.6 (8) |
| DENIS 1454−6604 | 16.90 | 13.06 | 3.84 | L3.5 (3) | <5 (3) | |

which was then trimmed. Numerous flat-field exposures obtained during evening twilight were combined to provide an accurate map of varying pixel sensitivities for each of the filters used. Images were then cleaned, and flat-field-corrected. A pipelined version of DOPHOT (Schechter, Mateo & Saha 1993) was used to obtain both aperture and point spread function (PSF) photometry.

The field of view of the cameras included numbers of relatively bright stars, and several of these were used as local standards, the exact choice depending on results for a given night and filter. Differential PSF magnitudes were found to exhibit less scatter than aperture–photometry magnitudes, and were therefore preferred. A least-squares method (Koen 2012) was used to tie photometry from different nights together. The zero-points in Table 2 provide some indication of the relative merits of the different nights: zero entries indicate that the particular night served as overall reference for the particular filter.

The differential, zero-point adjusted lightcurves are plotted in Figs 1–7.

## 3 DATA ANALYSES

It is perhaps worth remarking that for each of the data sets analysed below, the amplitude spectrum of one or more local comparison stars was also examined. Invariably the dominant peaks in these were at a much lower level (typically below 2 mmag) than seen in the spectra of the UCD. Ideally, peaks in amplitude spectra or periodograms should have been tested for statistical significance, but a generally applicable methodology to do this is not yet available.

### 3.1 Kelu-1

Fig. 8 shows amplitude spectra of the individual *I*-band runs logged in Table 2. Low-frequency power has been pre-whitened from the spectra by subtraction of second-order polynomials, and low-frequency sinusoids. Maxima near 13 d$^{-1}$ can be seen in the spectra for JD 245 4203−5. On some other nights maxima are sometimes at slightly higher frequencies ($\sim$15 d$^{-1}$, JD 245 3854, JD 245 4207−8), but the frequency resolution is poor.

The amplitude spectra of combined data from different nights are plotted in Fig. 9. In the case of the *I* band data from the last six successive nights were used to generate the spectrum in the panel labelled 'I0'. Observations in *R* were obtained during the last four of these nights, and the spectrum based on these is in panel 'R0'. (The corresponding window functions can be seen in Fig. 10: there is a fairly strong 1 d$^{-1}$ ambiguity, but other aliases are weak). Individual runs were detrended by subtraction of quadratic fits. Maxima in the panels labelled 'R0' and 'I0' are at very similar frequencies – 4.60 and 4.61 d$^{-1}$. If these are pre-whitened from the data, the residual spectra in panels R1 and I1 are obtained; maxima are at frequencies 12.28 and 6.04 d$^{-1}$, respectively. Further pre-whitening by these leads to the spectra in panels R2 and I2, with maxima at 20.91 and 13.28, respectively. The frequencies, with the corresponding amplitudes obtained by least-squares fitting, are listed in the first part of Table 3. The formal least-squares errors given in this, and the following tables, should be seen as indicative, rather than definitive, as the required statistical assumption of uncorrelated residuals (for one) is not met.

Some experimentation revealed that the $\sim$4.6 d$^{-1}$ periodicities which are prominent in both *I* and *R* are a consequence of the substantial low-frequency variability which is visible in the lightcurves obtained on JD 245 4207. The second part of Table 3 therefore shows the results of excluding data from that night. Only one peak in the *R*-band amplitude spectrum is convincingly above the noise level, at a frequency very close to the frequency of maximal power in *I*.

The results in Table 3 slightly refine the frequency detected by Clarke et al. (2002) to 13.38 d$^{-1}$. No other periodicities can reliably be extracted from the data (though it is noted in passing that 7.65 d$^{-1}$ is a 1 d$^{-1}$ alias of the subharmonic frequency 6.65 d$^{-1}$).

### 3.2 2M 1155−3727

Data published by Koen (2003) are presented (in slightly edited form) in the top five panels of Fig. 3; comparison with the last three panels shows a dramatic change in the amplitude of the variations. Koen (2003) found that these *I*-band brightness changes could be described by a sinusoid with a frequency of 3.031 d$^{-1}$ and an amplitude of 26 mmag. Given the closeness of the frequency to 3 d$^{-1}$, a typical value induced by differential extinction when observing objects with extreme colours, arguments were presented as to why the variability was most likely *not* due to this effect. The new measurements confirm that differential extinction does not play an important role in *I*-band observations of 2M 1155−3727.

The same cannot be said of data obtained in *R*. The gross variations in the last three sets of measurements in Fig. 4 can be modelled quite well by a sinusoid with a frequency of 2.000 64, indicative of probable substantial differential extinction. In Fig. 11, these differential magnitudes are plotted against zenith angle. Least-squares fits of straight lines are also shown. The fits were used to correct for the effects of airmass, and the results are plotted in Fig. 12. The analysis of the *R*-band data which follows is based on these pre-whitened data, which do not need any detrending.

The bottom three panels of Fig. 3 are replotted on an expanded scale in Fig. 13. Aside from the small amplitude compared to the earlier observations, it also appears that the time-scale of the variability is shorter – about 0.15 d (see particularly the bottom panel of Fig. 13), which implies a frequency of about 7 d$^{-1}$. Longer time-scale trends are also evident in the last two sets of measurements;

**Table 2.** The photometric observing log: $T_{exp}$ is the exposure time and $N$ the number of useful measurements. The last column is the estimated zero-point offset for the night, with respect to the 'best' reference night. The standard error of the zero-point is given in parentheses.

| Starting time (HJD 245 0000+) | Filter | $T_{exp}$ (s) | Run length (h) | $N$ | $\mu$ (S.E.) (mmag) |
|---|---|---|---|---|---|
| Kelu-1 | | | | | |
| 3532.2091 | *I* | 50 | 4.9 | 90 | 78 (5) |
| | *R* | 70–90 | 4.8 | 87 | 100 (3.2) |
| 3854.2623 | *I* | 80 | 4.1 | 58 | −125 (5) |
| | *R* | 120 | 4.0 | 61 | 0 |
| 4203.2699 | *I* | 120 | 8.7 | 219 | −75 (5) |
| 4204.3163 | *I* | 120–180 | 6.9 | 107 | 650 (5) |
| 4205.2501 | *I* | 90 | 9.0 | 111 | −136 (5) |
| | *R* | 150 | 8.8 | 100 | 41 (3) |
| 4206.2578 | *I* | 80–90 | 8.7 | 114 | −115 (5) |
| | *R* | 150–180 | 8.7 | 107 | 71 (3) |
| 4207.2595 | *I* | 80 | 8.6 | 113 | −57 (5) |
| | *R* | 150 | 8.6 | 111 | 116 (3) |
| 4208.2528 | *I* | 80–120 | 7.9 | 117 | 0 |
| | *R* | 150 | 5.6 | 78 | 120 (3) |
| 2M 1155−3727 | | | | | |
| 2759.2245 | *I* | 90 | 5.6 | 99 | −444 (4) |
| 2760.2420 | *I* | 100–120 | 1.7 | 50 | −419 (4) |
| 2761.2115 | *I* | 90 | 6.8 | 208 | −401 (4) |
| 2765.2233 | *I* | 80–120 | 6.4 | 161 | −252 (3) |
| 2766.2376 | *I* | 100 | 4.9 | 146 | −426 (3) |
| 4123.5291 | *I* | 70 | 2.1 | 32 | 0 (2) |
| | *R* | 120 | 2.1 | 32 | 0 |
| 5298.2563 | *I* | 180 | 9.2 | 72 | −5 (2) |
| | *R* | 240 | 9.0 | 69 | 228 (2) |
| 5299.2326 | *I* | 180 | 9.7 | 70 | 0 |
| | *R* | 240 | 9.5 | 62 | 247 (2) |
| 5300.2328 | *I* | 150–180 | 9.5 | 79 | 38 (3) |
| | *R* | 200–240 | 9.5 | 76 | 257 (2) |
| DENIS 1454−6604 | | | | | |
| 4552.4085 | *I* | 90–120 | 4.6 | 139 | −559 (3) |
| 4553.4190 | *I* | 90 | 5.7 | 70 | −530 (3) |
| | *R* | 150 | 5.7 | 67 | −204 (3) |
| 4554.4057 | *I* | 120 | 6.2 | 78 | −509 (2) |
| | *Z* | 90–120 | 6.3 | 78 | 0 |
| 4555.4073 | *I* | 90–120 | 6.1 | 68 | −565 (2) |
| | *R* | 180 | 3.7 | 23 | −223 (2) |
| | *Z* | 120–180 | 4.2 | 44 | 338 (1) |
| 4643.2168 | *I* | 90–120 | 4.5 | 75 | −547 (3) |
| | *R* | 150–200 | 2.6 | 30 | 0 |
| 4646.2049 | *I* | 120 | 2.9 | 35 | −494 (2) |
| | *Z* | 120 | 2.9 | 36 | −47 (1) |
| 4948.4149 | *I* | 120 | 6.1 | 78 | −595 (2) |
| | *Z* | 120–150 | 6.0 | 77 | −31 (1) |
| 4949.3699 | *I* | 120 | 5.2 | 34 | 0 |
| | *R* | 240 | 5.7 | 35 | 371 (3) |
| | *Z* | 150 | 5.5 | 37 | −133 (1) |

the *I*-band data were therefore pre-whitened by linear fits prior to analysis.

The study which follows is based on the detrended data from the last three nights. For each of the two filters data for all three nights were combined, in order to improve the frequency resolution. The *I*-band window function is plotted in Fig. 14; the window function of the *R*-band observations is very similar.

As in Fig. 9, the two sets of amplitude spectra (i.e. for *R* and *I*) are presented in a single diagram (Fig. 15) in order to facilitate comparison. The panels of the figure are labelled with the filter

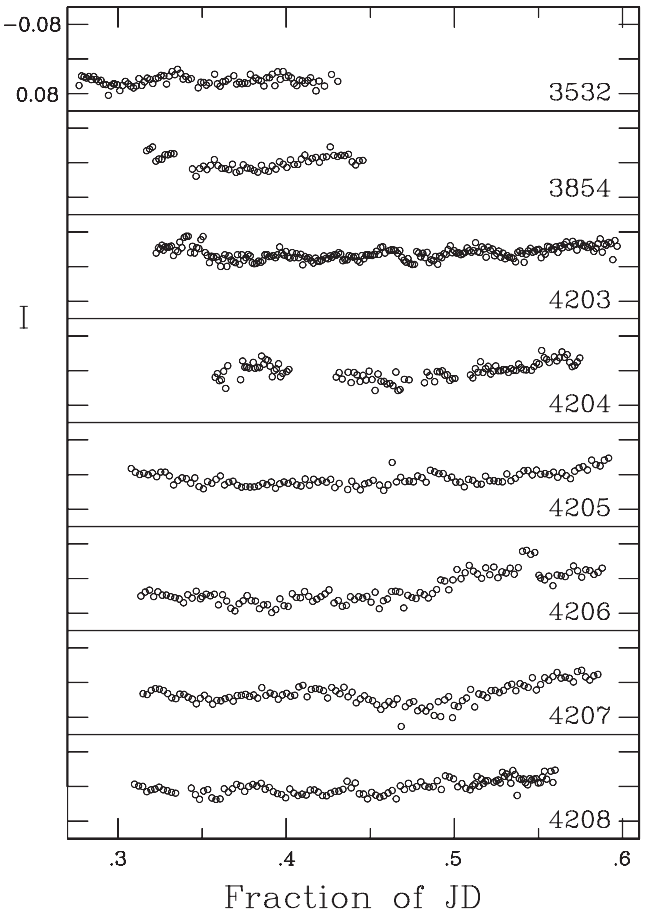


**Figure 1.** The *I*-band lightcurves of Kelu-1. Panels are labelled with the last four digits of the Julian Date on which data were obtained. Note that the vertical scales are all the same, so that changes in the mean levels and/or level of variability can be clearly seen.

names, and the number of pre-whitened sinusoids, as in Fig. 9 (see the description above). Frequencies and amplitudes corresponding to the highest peak in each of the panels are listed in Table 4; the amplitudes were obtained by least-squares fitting sinusoids with the dominant frequencies to the data.

Given the visual impression in Fig. 13 it is no surprise that the *I*-band spectrum shows a prominent peak at 6.98 $d^{-1}$ (and its 1 $d^{-1}$ alias). If this is pre-whitened from the data, an alias pattern of three peaks centred on 2.92 $d^{-1}$ becomes evident. The *R*-band data are dominated by a 3 $d^{-1}$ feature; this is close to the length of the individual runs, but the inspection of Fig. 12 suggests real variability on this time-scale. Note also that the third frequency extracted from the *R* data is less than two standard errors from the most prominent frequency in *I*.

The strong alias of the 6.98 $d^{-1}$ frequency in panel I0 is at 6.00 $d^{-1}$, which is close to twice the frequency 3.03 $d^{-1}$ found in the earlier observations of the UCD by Koen (2003).

It is concluded that

(i) There is a persistent periodicity of 3.44 or 4.00 h in the latest observations of 2M 1155−3727, clearly seen in *I*, and possibly present at a much lower level in *R*. Physically, the latter period is the more plausible, as it is exactly half the period previously measured in the object. A reasonable explanation for the difference in periods between the two epochs of observations is that a single local feature on the surface of the UCD has been replaced by two

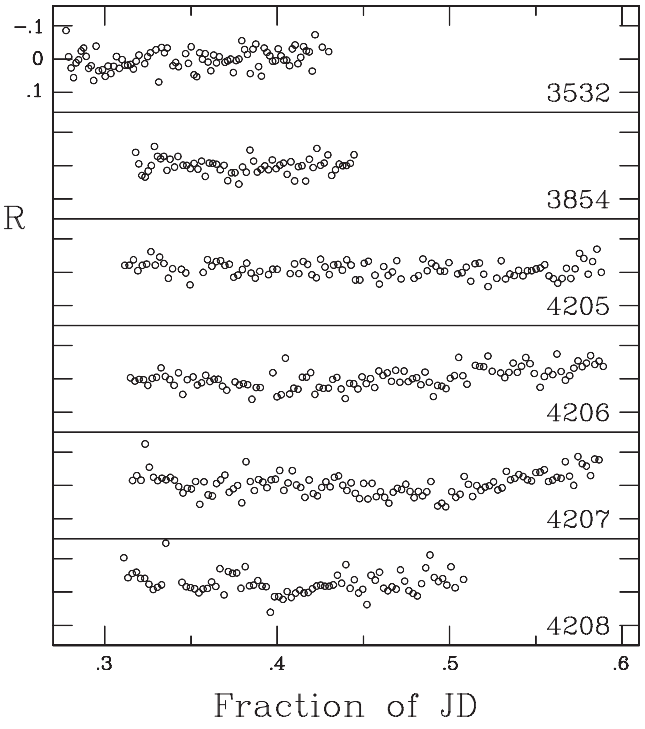


**Figure 2.** As for Fig. 1, but showing the *R*-band lightcurves of Kelu-1.

features separated by about 180°. ['Feature' in this context could be either a dark magnetically induced spot, or a large local irregularity in the dusty atmosphere (often referred to as 'weather') – see e.g. Goldman 2005.] There is no ready explanation for why the *R*-band variability is more pronounced at double the *I*-band period.

(ii) Although 2M 1155−3727 was discovered in the course of a survey of the young (∼10 Myr) TW Hydrae association (Gizis 2002), the object has very different spatial motion from confirmed members [compare *UVW* values in Seifahrt et al. (2010) and Zuckerman & Song (2004)]. This means that it is not necessarily young – note also that Faherty et al. (2012) did not place it amongst 'low gravity' objects. Accretion hot spots are therefore probably less likely than dark magnetically induced spots, or large-scale 'weather' features on the surface.

(iii) The very accurate measurement of the projected rotational velocity by Blake et al. (2010), namely $v \sin i = 13.6 \pm 0.3$ km s$^{-1}$, can be used together with the likely rotation period of 8 h to place the limit $R \geq 6.2 \times 10^9 \approx 0.9 R_J$ on the radius of the object. Conversely, if the canonical $R = R_J$ is assumed, an inclination angle of about 60° follows.

(iv) It is conceivable that $f = 2.93\,\mathrm{d}^{-1}$ corresponds to the strong periodicity in the earlier *I*-band observations. The dominant frequency in the *R*-band data is also at $3\,\mathrm{d}^{-1}$.

(v) Given the absence of any corresponding power excess at $10.67\,\mathrm{d}^{-1}$ in *I*, this feature in *R* is probably due to noise.

(vi) There is also longer time-scale variability in this UCD, as evidenced by the trends visible in the lower two panels of Fig. 13, and the different nightly mean levels in Figs 3 and 13 (note the different vertical plotting scales in the latter diagram).

### 3.3 DENIS 1454−6604

Persistent sinusoidal variability with a period of about 2.5 h can clearly be seen in the *I*-band (Fig. 5) and *Z*-band (Fig. 7) data.

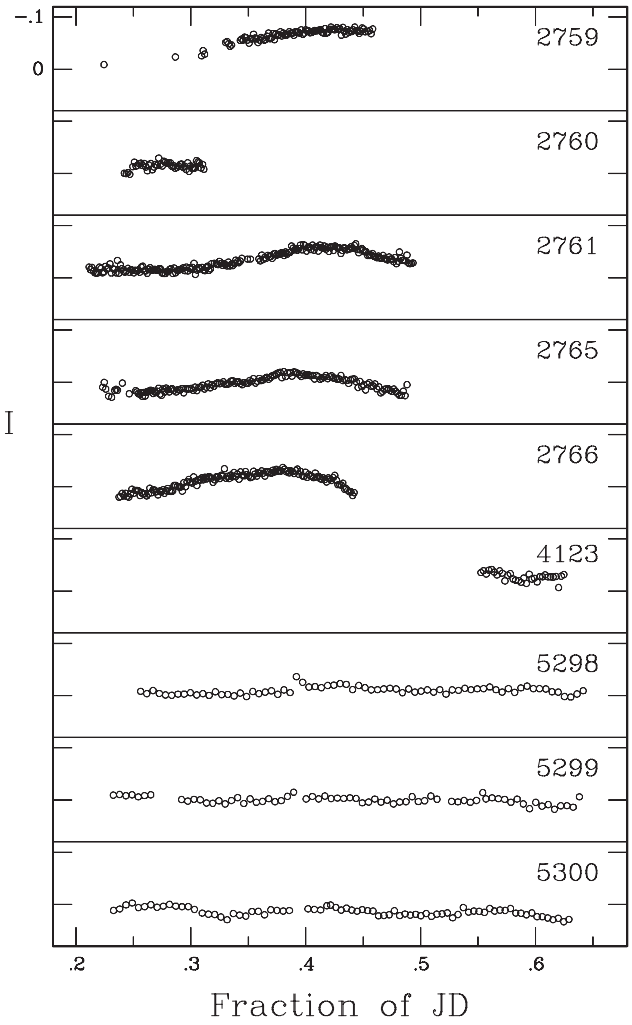


**Figure 3.** As for Fig. 1, but showing the *I*-band lightcurves of 2M 1155−3727.

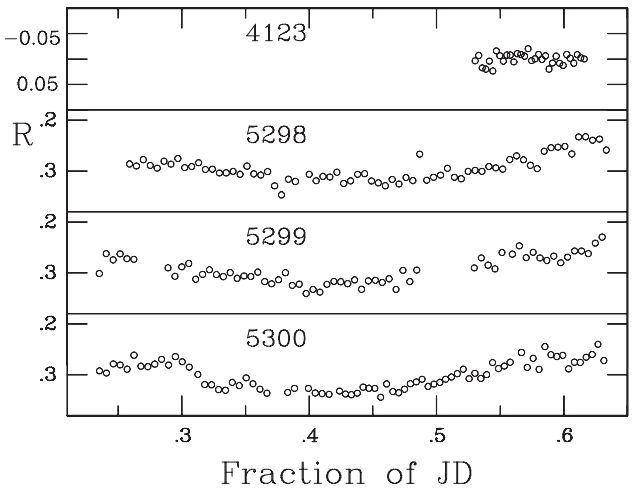


**Figure 4.** The *R*-band lightcurves of 2M 1155−3727. Panels are labelled with the last four digits of the Julian Date on which data were obtained. Note that although the vertical widths of all the panels are the same, the zero-point in the top panel is different, since the UCD was considerably brighter during this night.

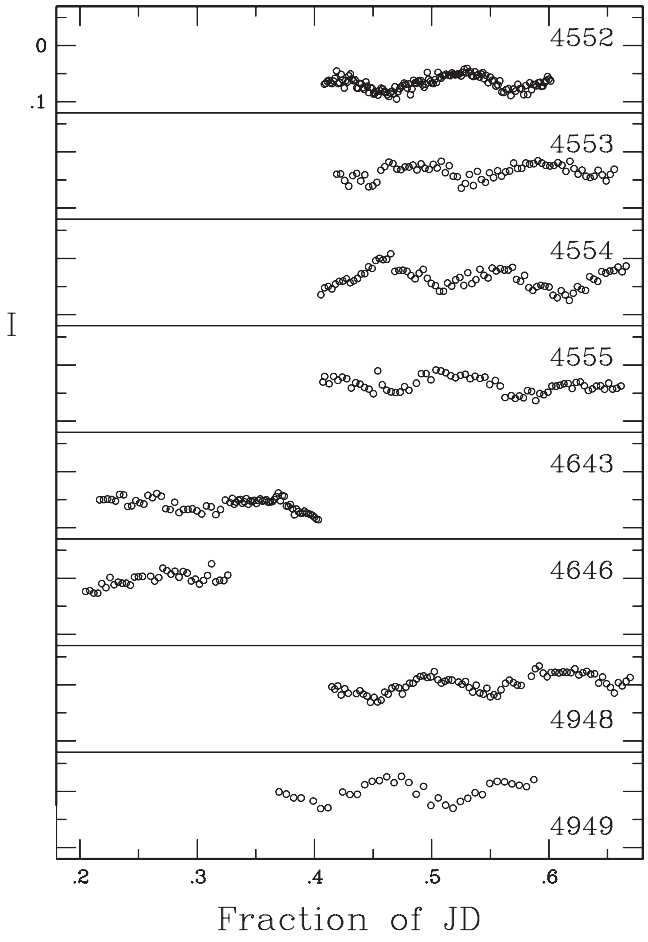


**Figure 5.** As for Fig. 1, but showing the *I*-band lightcurves of DENIS 1454−6604.

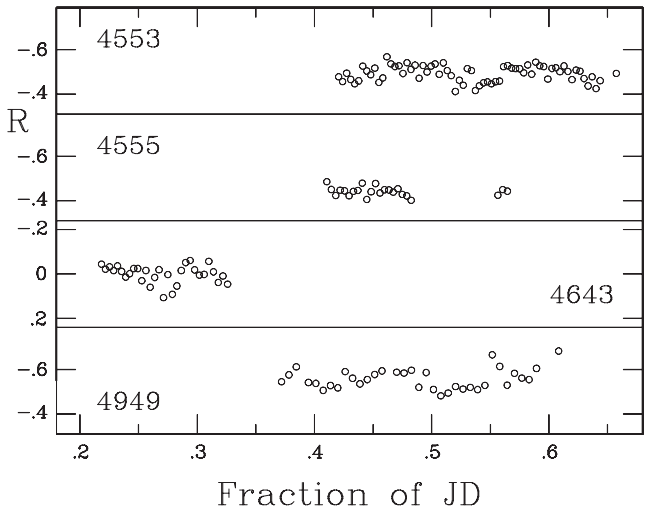


**Figure 6.** The *R*-band lightcurves of DENIS 1454−6604. Panels are labelled with the last four digits of the Julian Date on which data were obtained. Note that although the vertical widths of all the panels are the same, the zero-point in the panel third from the top is different, since the UCD was considerably fainter during this night.

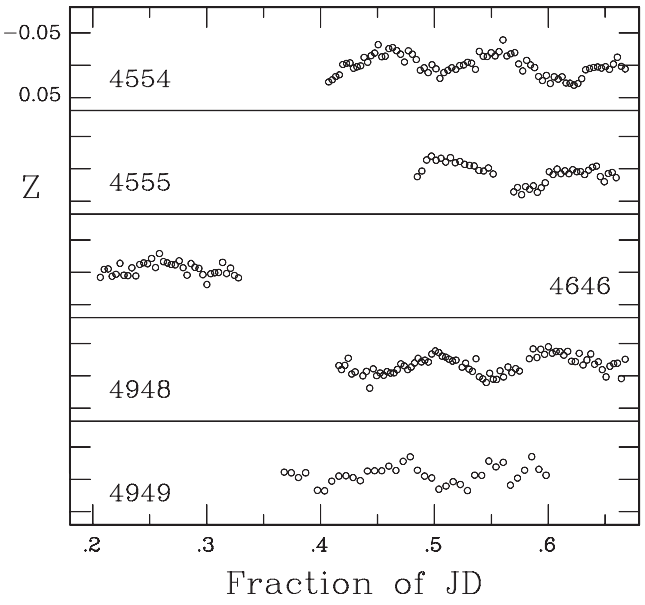


**Figure 7.** As for Fig. 1, but showing the *Z*-band lightcurves of DENIS 1454−6604.

**Table 3.** The most prominent sinusoidal components in observations of Kelu-1. The *R*-band data from the last four nights, and the *I*-band data from the last six, were respectively combined to derive the results in the first part of the table. All individual runs were first detrended by subtracting quadratic fits. Quantities in the second line were derived from the residuals after pre-whitening by sinusoids with properties given in the first line; results in the third line were obtained after pre-whitening by $f_1$ and $f_2$. Formal standard errors are given in parentheses. Residual standard deviations are denoted by $\sigma$. The second set of results were obtained similarly, but the data from JD 245 4207 were excluded.

| *R* | | | *I* | | |
|---|---|---|---|---|---|
| Frequency ($d^{-1}$) | Amplitude (mmag) | $\sigma$ (mmag) | Frequency ($d^{-1}$) | Amplitude (mmag) | $\sigma$ (mmag) |
| 4.60 (0.04) | 5.1 (1.3) | 18.6 | 4.61 (0.01) | 6.4 (0.7) | 12.5 |
| 12.28 (0.04) | 5.0 (1.3) | 18.3 | 6.04 (0.01) | 5.3 (0.6) | 12.4 |
| 20.91 (0.04) | 5.0 (1.3) | 17.9 | 13.28 (0.01) | 4.6 (0.6) | 12.0 |
| 13.29 (0.04) | 6.7 (1.5) | 18.0 | 13.27 (0.01) | 5.5 (0.7) | 12.5 |
| | | | 5.53 (0.01) | 5.0 (0.6) | 12.0 |
| | | | 7.65 (0.02) | 4.0 (0.6) | 11.6 |

**Table 4.** The most prominent sinusoidal components in the last three nights of observations of 2M 1155−3727. The *I*-band data were first detrended by subtracting linear fits to individual nights, while the *R*-band data in Fig. 12 were used. An alternative alias of the dominant *I*-band frequency is listed in the second line of the table. Quantities in the third line were derived from the residuals after pre-whitening by sinusoids with properties given in the first line; results in the last line were obtained after pre-whitening by $f_1$ and $f_2$. Residual standard deviations are denoted by $\sigma$. Formal standard errors are given in parentheses.

| *R* | | | *I* | | |
|---|---|---|---|---|---|
| Frequency ($d^{-1}$) | Amplitude (mmag) | $\sigma$ (mmag) | Frequency ($d^{-1}$) | Amplitude (mmag) | $\sigma$ (mmag) |
| 3.04 (0.02) | 12.2 (1.2) | 11.9 | 6.98 (0.02) | 5.4 (0.5) | 5.2 |
| | | | 6.00 (0.02) | 5.0 (0.5) | 5.4 |
| 10.70 (0.05) | 5.3 (1.1) | 11.3 | 2.92 (0.03) | 3.0 (0.4) | 4.7 |
| 7.10 (0.07) | 4.0 (1.1) | 10.9 | 6.60 (0.05) | 2.1 (0.4) | 4.5 |

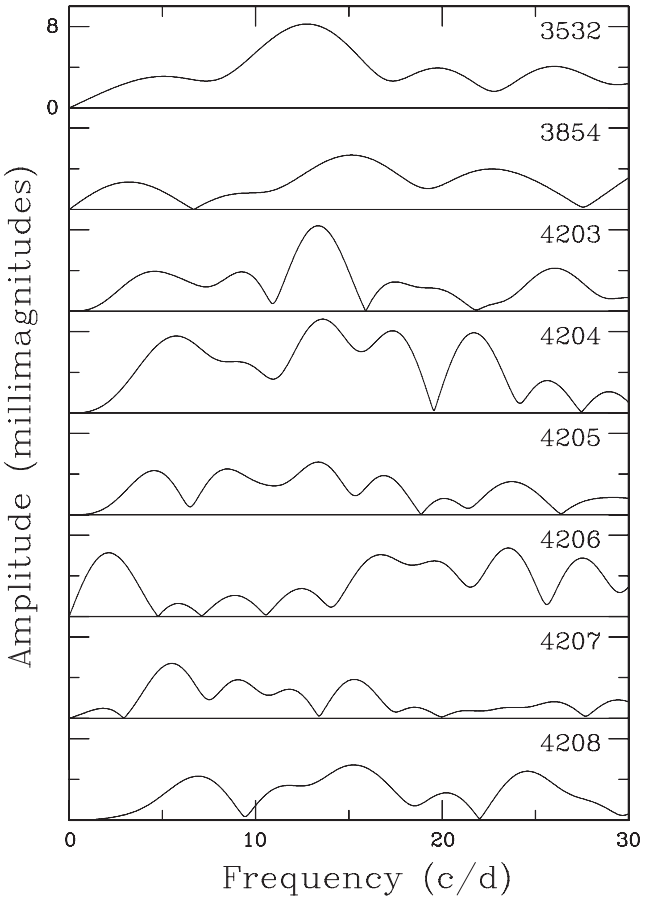


**Figure 8.** Amplitude spectra, all plotted on the same scale, of the individual *I*-band runs on Kelu-1. Some low-frequency ($f < 10\,\mathrm{d}^{-1}$) power has been removed by detrending, and by subtraction of low-frequency sinusoids. Panel labels are the last four digits of the Julian Dates of the observations.

There are also fairly large longer term changes in the mean level – compare, for example, the *I*-band light curves obtained on JD 245 4643 and JD 245 4646. Interestingly the mean levels of the two short *R*-band runs from the same two nights do not differ much (Fig. 6); neither is there much variation in the nightly means of the *Z*-band measurements plotted in Fig. 7.

Observations were made at three epochs – JD 245 4552−245 4555 (1); JD 245 4643−245 4646 (2); and JD 245 4948−245 4949 (3). In what follows data from a given epoch are combined, and abbreviations such as e.g. 'Z (e3)' are used to refer to the *Z*-band data obtained during the third of the epochs. In the case of the *R* band, measurements made on JD 245 4555 and JD 245 4643 are few, and those two runs are not used. Also, I (e2) and Z (e2) are much less extensive than I (e1), I (e3) and Z (e1), Z (e3), and are hence not analysed.

Since there are slight trends in some of the individual data sets, all data were linearly detrended before frequency analysis. The amplitude spectra are plotted in Fig. 16. Given the prominence of the $\sim 10\,\mathrm{d}^{-1}$ variations in Figs 5 and 7, it comes as no surprise that maximal power in the spectra is centred at about this frequency. Fig. 17 shows the residual spectra after pre-whitening by the frequencies corresponding to the maxima in Fig. 16, and Table 5 lists the frequencies and amplitudes of interest.

An inspection of the table shows good agreement between the results from the different runs and filters. The best determination of the principal frequency is $9.328 \pm 0.008\,\mathrm{d}^{-1}$ ($P = 2.573 \pm 0.002$ h).

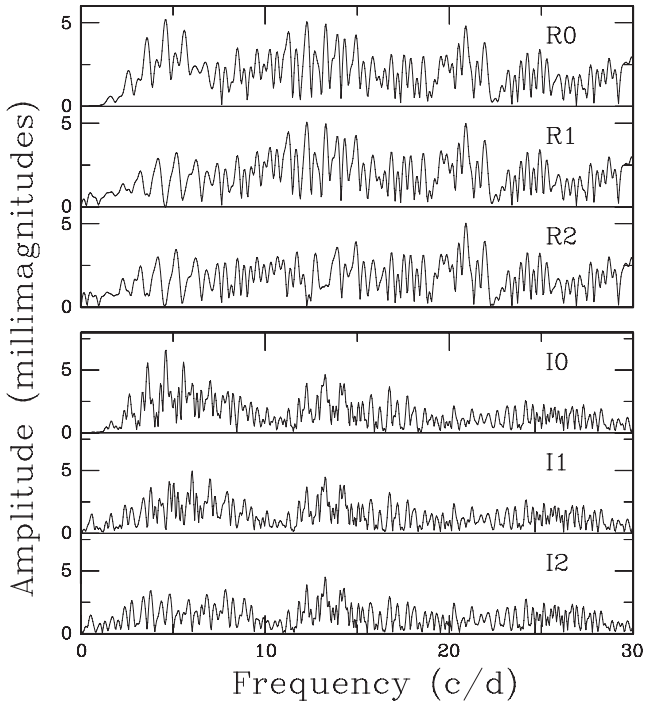


**Figure 9.** Amplitude spectra of the combined last four *R*-band runs (top panels) and combined last six *I*-band runs (bottom panels) on Kelu-1. Individual runs have been pre-whitened by subtraction of quadratic fits. Panel labels indicate the filter names, followed by the number of frequencies pre-whitened form the data. For example, the spectrum labelled 'I2' is based on the combined *I*-band data, from which the two peak frequencies in panels I0 and I1 have been pre-whitened.

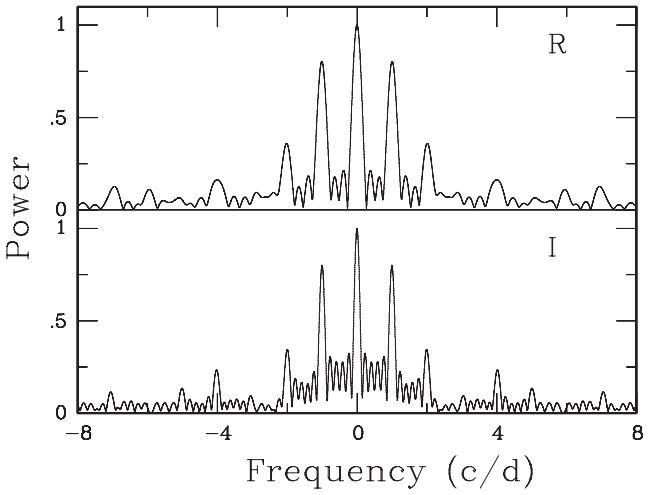


**Figure 10.** The window functions of the data used to calculate the spectra in Fig. 9.

Amplitudes in *I* and *Z* are quite similar, and although the *R*-band determination is very uncertain, comparison of Fig. 6 with Figs 5 and 7 does suggest that variations may be more pronounced at the shorter wavelength.

The good correspondence between the secondary frequencies is also interesting. In the case of the two exceptions [R (e2) and Z (e3)] there are also prominent features at 4.6 and $4.9\,\mathrm{d}^{-1}$, respectively. The most likely explanation may be that these lower frequencies correspond to the subharmonic $4.66\,\mathrm{d}^{-1}$ of the dominant frequency.

**Table 5.** The most prominent sinusoidal components in the amplitude spectra of DENIS 1454−6604, as shown in Figs 16 and 17. All individual runs were first detrended by subtracting linear fits. Residual standard deviations are denoted by $\sigma$. Formal standard errors are given in parentheses.

| Data set | Raw data (Fig. 16) | | | Pre-whitened data (Fig. 17) | | |
|---|---|---|---|---|---|---|
| | Frequency ($d^{-1}$) | Amplitude (mmag) | $\sigma$ (mmag) | Frequency ($d^{-1}$ | Amplitude (mmag) | $\sigma$ (mmag) |
| I (e1) | 9.328 (0.008) | 14.2 (0.7) | 8.9 | 4.69 (0.02) | 4.7 (0.6) | 8.3 |
| I (e3) | 9.35 (0.03) | 16.6 (1.0) | 7.4 | 4.86 (0.13) | 3.5 (0.9) | 7.0 |
| R (e1) | 9.2 (0.4) | 32 (4.8) | 28.2 | 17.28 (1.3) | 8 (4.8) | 27.5 |
| R (e3) | 8.8 (0.7) | 30 (10) | 40.1 | 4.3 (0.9) | 22 (8.8) | 36.6 |
| Z (e1) | 9.36 (0.03) | 17.4 (1.1) | 8.5 | 4.23 (0.06) | 7.0 (0.9) | 7.1 |
| Z (e3) | 9.33 (0.04) | 14.3 (1.1) | 8.6 | 14.56 (0.15) | 3.4 (1.1) | 8.3 |

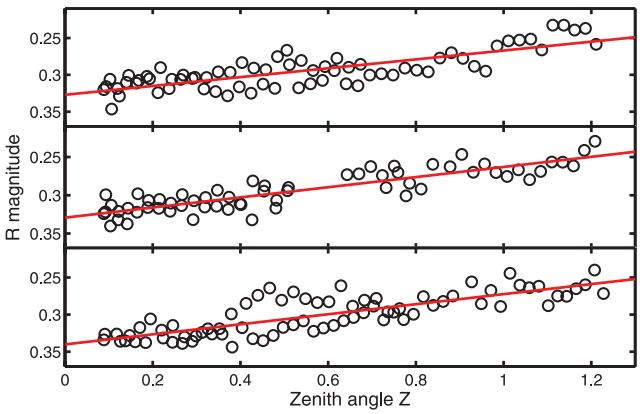


**Figure 11.** The dependence on the zenith angle of the differentially corrected *R*-band magnitudes of 2M 1155−3727 (Fig. 4). From top to bottom, data are from JD 245 5298, 245 5299 and 245 5300, respectively. Also shown are linear least-squares fits.

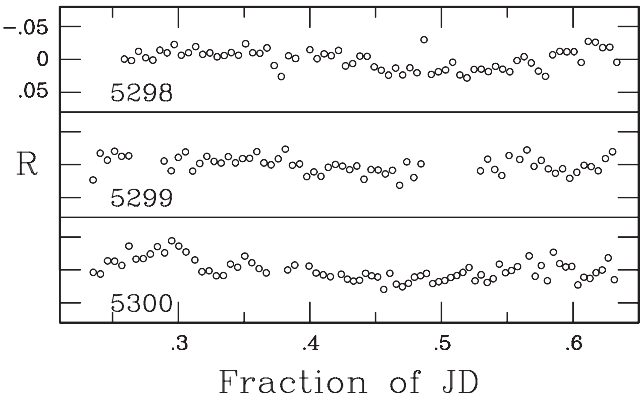


**Figure 12.** As in the lower three panels of Fig. 4, but corrected for the dependence on zenith angle demonstrated in Fig. 11. The vertical scales on the three panels are the same.

If so, then a physical explanation of the variability could be two symmetrically placed features on the surface of the UCD, giving rise to rotational modulation with a period of 5.15 h.

## 4 CLOSING REMARKS

(i) It is clear from Fig. 8 that the variability of Kelu-1 evolves on a time-scale of days, definitely in amplitude, and possibly also in frequency.

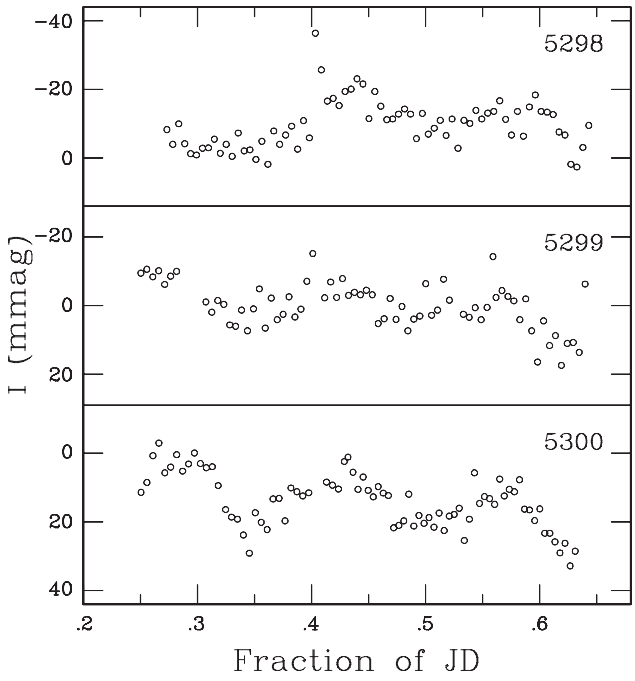


**Figure 13.** The last three nights' *I*-band observations of 2M 1155−3727, plotted on an expanded vertical scale in order to show more clearly the detail of the small amplitude variations. Note the vertical offsets of the three panels from each other.

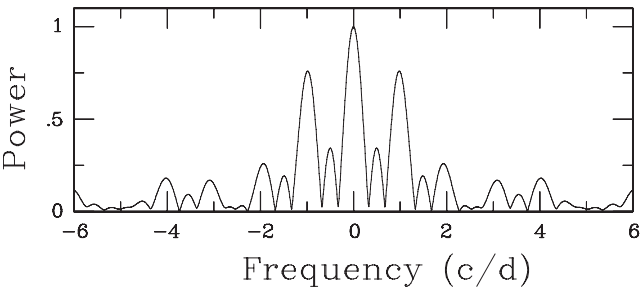


**Figure 14.** The window function of the data in Fig. 13. The window function of the *R*-band data in Fig. 12 is virtually identical, since observations in *R* and *I* were contemporaneous.

(ii) There has been a marked change in the variability of 2M 1155−3727, both in amplitude and period. The change in period may be most plausibly explained by a change from a one local spot (or 'weather' pattern) configuration, to two features separated by 180°.

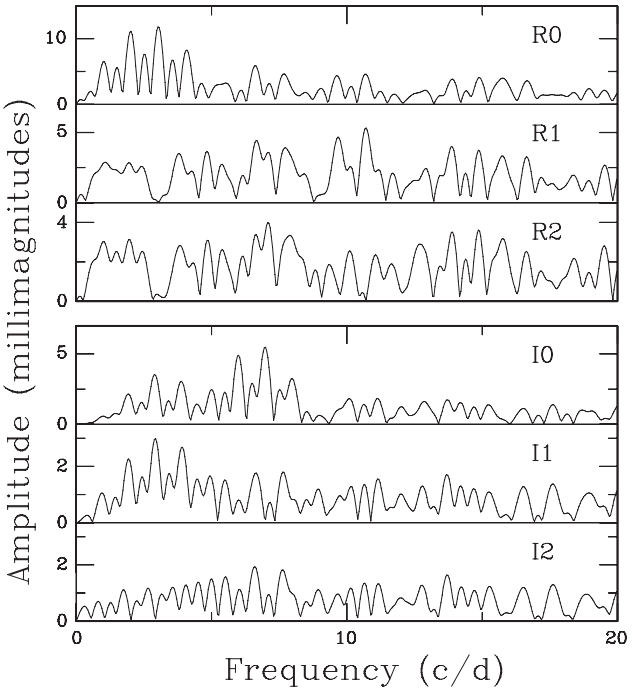


**Figure 15.** As for Fig. 9, but for the combined last three *R*-band runs, and last three *I*-band runs, on 2M 1155−3727.

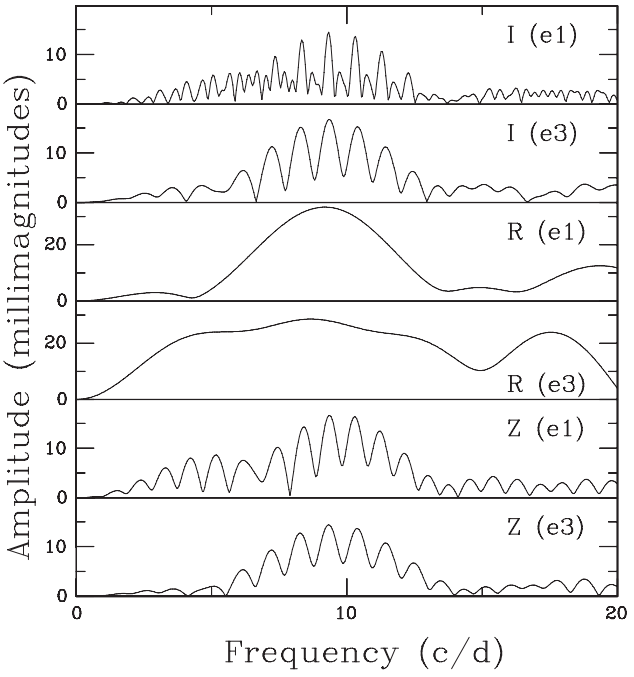


**Figure 16.** Amplitude spectra of the DENIS 1454−6604 observations. Panels are labelled with filter names, followed by the epoch of the observations. Note that the *I* and *Z* data are plotted on the same vertical scale, which is different from the scale used for *R*.

(iii) A sustained 2.6 h periodicity is evident in light curves of DENIS 1454−6604. In the context of UCDs, the amplitude is fairly large, in excess of 1 per cent. It is possible that a subharmonic of the primary periodicity is also present in the data – this would imply a rotation period of 5.2 h. Determination of $v \sin i$ of this object would be useful.

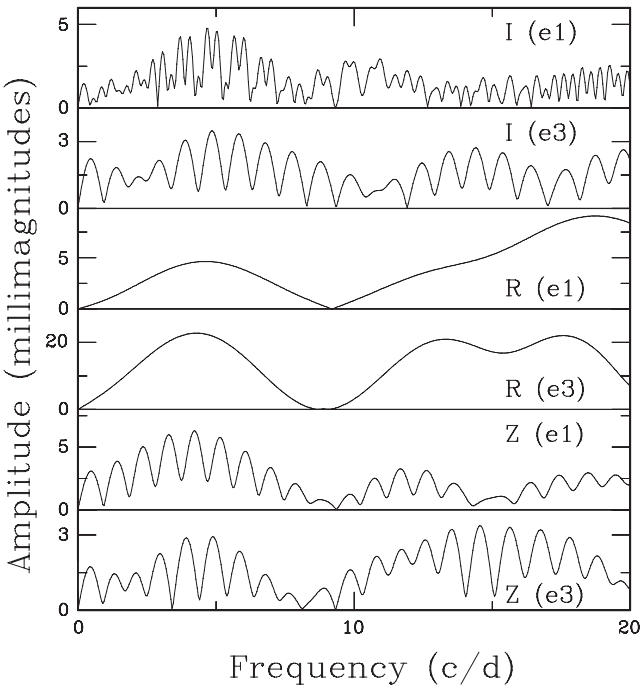


**Figure 17.** As for Fig. 16, but for the residual DENIS 1454−6604 data, after pre-whitening by the frequencies of maximal power in that figure. Note the different vertical scales on the different panels.

(iv The *R*-band amplitudes may be substantially different from that in *I* in the case of DENIS 1454−6604. Unfortunately the observations of the object in the former filter are rather sparse – obtaining extensive *R*-band data of this UCD would certainly be worthwhile. Comparison of amplitudes of 2M 1155-3727 is complicated by the fact that different dominant frequencies are seen in the two filters.

(v) There are substantial changes in the mean brightness levels of the UCDs, on time-scales of days and/or longer. The one exception seems to be the *Z*-band observations of DENIS 1454−6604.

## ACKNOWLEDGMENTS

The author is grateful to those maintaining the Simbad data base in Strasbourg, France; and to those responsible for the DENIS and 2MASS catalogues. He also appreciates allocation of telescope time by SAAO, and financial support from the South African National Research Foundation. Incisive comments by the referee, Dr Fraser Clarke, led to a much improved text.

This paper was completed while visiting the Space Sciences Laboratory at the University of California, Berkeley. The author is grateful to the Experimental Astrophysics Group, and in particular to Prof. Oswald Siegmund and Dr Barry Welsh, for their hospitality.

## REFERENCES

Antonova A., Doyle J. G., Hallinan G., Bourke S., Golden A., 2008, A&A, 487, 317
Audard M. et al., 2007, A&A, 471, 63
Basri G., Mohanty S., Allard F., Hauschildt P. H., Delfosse X., Martín E. L., Forveille T., Goldman B., 2000, ApJ, 538, 363
Berger E., 2006, ApJ, 648, 629
Blake C. H., Charbonneau D., White R. J., 2010, ApJ, 723, 684
Clarke F., Tinney C. G., Covey K. R., 2002, MNRAS, 332, 361
Clarke F., Tinney C. G., Hodgkin S. T., 2003, MNRAS, 341, 239

Dahn C. C. et al., 2002, AJ, 124, 1170
Epchtein N. et al., 1999, A&A, 349, 236 (DENIS catalogue)
Faherty J. K., Burgasser A. J., Cruz K. L., Shara M., Walter F. M., Gelino C. R., 2009, AJ, 137, 1
Faherty J. K. et al., 2012, ApJ, 752, 56
Gelino C. R., Kulkarni S. R., Stephens D. C., 2006, PASP, 118, 611
Gizis J. E., 2002, ApJ, 575, 484
Goldman B., 2005, Astron. Nachr., 326, 1059
Goldman B., Pitann J., Zapatero Osorio M. R., Bailer-Jones C. A. L., Béjar V. J. S., Caballero J. A., Henning Th., 2009, A&A, 502, 929
Koen C., 2003, MNRAS, 346, 473
Koen C., 2012, submitted
Liebert J., Gizis J. E., 2006, PASP, 118, 659
Littlefair S. P., Dhillon V. S., Marsh T. R., Shahbaz T., Martín E. L., 2006, MNRAS, 370, 1208
Liu M. C., Leggett S. K., 2005, ApJ, 634, 616
Mohanty S., Basri G., 2003, ApJ, 583, 451
Patten B. M. et al., 2006, ApJ, 651, 502
Phan-Bao N. et al., 2008, MNRAS, 383, 831
Reiners A., Basri G., 2008, ApJ, 684, 1390
Schechter P. L., Mateo M., Saha A., 1993, PASP, 105, 1342
Seifahrt A., Reiners A., Almaghrbil K. A. M., Basri G., 2010, A&A, 512, 37
Skrutskie M. F. et al., 2006, AJ, 131, 1163 (2MASS catalogue)
Zapatero Osorio M. R., Caballero J. A., Béjar V. J. S., 2005, ApJ, 621, 445
Zuckerman B., Song I., 2004, ARA&A, 42, 685

This paper has been typeset from a TEX/LATEX file prepared by the author.